THE JOURNAL OF COMPARATIVE NEUROLOGY 461:415–428 (2003)

Quantitative Morphologic Classification of Layer 5 Neurons from Mouse Primary Visual Cortex

ARETI TSIOLA,* FARID HAMZEI-SICHANI, ZITA PETERLIN, AND RAFAEL YUSTE
Department of Biological Sciences, Columbia University, New York, New York 10027

ABSTRACT

The understanding of any neural circuit requires the identification and characterization of all its components. Morphologic classifications of neurons are, therefore, of central importance to neuroscience. We use a quantitative method to classify neurons from layer 5 of mouse primary visual cortex, based on multidimensional clustering. To reconstruct neurons, we used Golgi impregnations and biocytin injections, as well as DiOlistics, a novel technique of labeling neurons with lipophilic dyes. We performed computerized 3-D reconstructions of 158 layer 5 cells to measure a series of morphologic variables. Principal component analysis and cluster analysis were used for the classification of cell types. Five major classes of cells were found: group 1 includes large pyramidal neurons with apical dendrites that reach layer 1 with an apical tuft; group 2 consists of short pyramidal neurons and large multipolar cells with "polarized" dendritic trees; group 3 is composed of less extensive pyramidal neurons; group 4 includes small cells; and group 5 includes another set of short pyramidal neurons in addition to "atypically oriented" cells. Our sample included a relatively homogeneous group of 27 neurons that project to the superior colliculus, which clustered mainly in group 1, thus supporting the validity of the classification. Cluster analysis of neuronal morphologies provides an objective method to quantitatively define different neuronal phenotypes and may serve as a basis for describing neocortical circuits. J. Comp. Neurol. 461:415–428, 2003.

Indexing terms: biocytin; DiOlistics; two-photon; principal component; cluster analysis

Despite over a century of continuous experimental effort, no unitary theory of cortical function has emerged (Mountcastle, 1998). This can be attributed to the astronomical number of cortical neurons and the apparent complexity of their connectivity. In fact, although there has been great progress in defining cell types and deciphering some of their projections (Ramón y Cajal, 1904; Lorente de Nó, 1922; Szentagóthai, 1978; Gilbert and Wiesel, 1983; Martin and Whitteridge, 1984; Lund, 1988; Gupta et al., 2000), even the number of classes of cortical neurons is still unknown and is subject to debate (Douglas and Martin, 1998; Somogyi et al., 1998). According to some investigators, there are essentially seven types of neurons in the cortex (Sholl, 1956), whereas according to others, there may be as many as several hundred or a thousand (Solnick et al., 1984; Crick and Asanuma, 1986; Stevens, 1998). The exact catalog of neocortical cell types and the description of their connections appear essential for the elucidation of their functions. For example, in a recent study in the retina, many types of amacrine cells were identified on the basis of dendritic branching (MacNeil et al., 1999) and each cell type is in principle thought to have a specific pattern of connectivity and function. It is likely that a similar situation would occur in the neocortex and that each different class of neuron could implement a particular circuit function.

Previous morphologic classifications of cortical neurons have been qualitative, i.e., neurons were grouped according to morphologic criteria that were subjectively chosen

Grant sponsor: National Eye Institute; Grant number: EY13237; Grant sponsor: John Merck Fund.

Mr. Hamzei-Sichani's present address is Department of Physiology and Pharmacology, State University of New York, Brooklyn, New York 11203.

*Correspondence to: Areti Tsiola, Department of Biological Sciences, Columbia University, MC 2436, 1212 Amsterdam Avenue, New York, NY 10027. E-mail: at181@columbia.edu

Received 21 May 2002; Revised 17 October 2002; Accepted 23 December 2002

DOI 10.1002/cne.10628

Published online the week of May 19, 2003 in Wiley InterScience (www.interscience.wiley.com).

to be important (Lorente de Nó, 1922). In some cases, specific types of neurons have been described in combination with the physiological and chemical properties of these cells, but there has been no objective classification of cortical neurons based on morphologic criteria that most investigators would agree upon. Similar to the practice of zoology, the capacity of a trained investigator to recognize specialized patterns in order to classify different species and to make sense of an apparently random assortment of forms, cannot be underestimated. At the same time, the drawback of this approach is that the morphologic criteria that may be important to one researcher may not be so important to another. This is an essential problem that historically has affected cortical anatomy (Stevens, 1998).

Like in many fields of biology, multidimensional quantitative comparisons of neuronal phenotypes or genotypes could provide an objective and universal system to classify them into groups. One approach is the use of cluster analysis (Nadol et al., 1990; Kolb et al., 1994; Cauli et al., 2000; Tamas et al., 2000), which refers to mathematical methods that group objects in a data set based on their degree of similarity in a multidimensional space. Cluster analysis produces a dendrogram that represents the various classes and subclasses. The linkage distance between cases (cells) is plotted on the y-axis in arbitrary units and is inversely proportional to the degree of similarity among them.

Our goal was to define morphologic classes of cortical neurons in layer 5 of the mouse visual cortex using quantitative criteria. Layer 5 was chosen for several reasons. It is the main output layer of the cortex; it is easy to define even without counterstaining; and its large pyramidal cells have been subject to intense physiological, biophysical, anatomic, and theoretical studies in the past decades. In addition, we took advantage of the fact that there is a population of layer 5 pyramidal neurons that project to the superior colliculus and that can be retrogradely labeled by using fluorescence microspheres, as a control for our final morphologic classification scheme. We first stained neurons in the primary visual cortex (V1) of the mouse by using Golgi impregnations, biocytin injections, as well as DiOlistics, a novel technique of labeling neurons with lipophilic dyes (Gan et al., 2000). We then reconstructed 158 cells to obtain their three-dimensional (3-D) structure and created a list of variables that reflect their somatic and dendritic morphologies. To create an objective classification scheme, we chose a combination of cluster analysis with principal component analysis (PCA) to simplify the data set and, more importantly, to decrease the bias that could be introduced by the set of variables themselves. We find two broad groups of neurons, with and without apical tufts extending immediately below the pia mater. The tuft-less cells are divided into four major groups. One class of cells has polarized dendritic arbors of nonpyramidal and pyramidal morphologies. Pyramidal neurons with much less elaborate basal and apical dendritic arbors fall into another category. A third group of tuft-less cells consists of purely small cells. The fourth group includes "short" pyramidal cells and nonpyramidal ones with dendrites oriented atypically, i.e., diagonally through the cortical layers. Interestingly, the superior colliculus–projecting cells fell mostly within the first cluster, supporting the validity of the method.

MATERIALS AND METHODS

All experiments were carried out in accordance with the NIH Guide for the Care and Use of Laboratory Animals (NIH publication no. 86-23, revised 1987).

Preparation of mice and material

C57BL/6 mice, postnatal days (PND) 13 to 21 were anesthetized with 120 mg/kg ketamine, 10 mg/kg xylazine (i.m. or i.p.). Brains were removed quickly and placed in cold (4°C) high-sucrose artificial cerebrospinal fluid (ACSF) containing the following: 26 mM $NaHCO_3$, 1 mM NaH_2PO_4, 10 mM dextrose, 3 mM KCl, 206 mM sucrose, 2 mM $MgSO_4$, 2 mM $CaCl_2$. Slices were cut in the coronal plane 300 μm thick on a Vibratome (Leica) and incubated at room temperature (RT) in a submerged chamber containing oxygenated (95% CO_2, 5% O_2) nonsucrose ACSF (126 mM NaCl, 26 mM $NaHCO_3$, 1.1 mM NaH_2PO_4, 10 mM dextrose, 3 mM KCl, 2 mM $MgSO_4$, 2 mM $CaCl_2$).

In the cases where fixed tissue was stained, anesthetized animals were initially perfused intracardially with physiological saline (0.9% NaCl) at 4°C and then with fixative solution at RT. For Nissl staining, tissue was fixed in formalin, and for all other histologic procedures 4% paraformaldehyde in 0.1 M phosphate buffer (PB, pH 7.35) was used. The brain was removed quickly and kept in the same fixative solution overnight. For Golgi staining, brains were eventually embedded in paraffin. For histologic staining, brains were either embedded in paraffin and sectioned on a sliding microtome (AO Instrument Co.) at 90 μm, or were allowed to sink in 30% sucrose in 0.1 M PB at RT before being embedded in Tissue Tek (Sakura) to be sectioned at 30 μm on a cryostat (Bright Instrument Co.).

Nissl stains

Mounted sections were hydrated through a cold decreasing ethanol (EtOH) series into ddH_2O and incubated for approximately 5 minutes in a filtered 0.5% cresyl violet (Sigma) solution prepared in acetate buffer (0.1 M, pH 3.5). The sections were differentiated and dehydrated in 95% and 100% EtOH, cleared in the xylene-substitute Microclear (Thomas Scientific), and cover-slipped with Permount (Fisher Scientific).

Cytochrome oxidase

For cytochrome oxidase staining, sections were incubated in a solution containing 0.03% cytochrome C, 0.01% catalase, and 0.05% DAB (Sigma) prepared in phosphate-buffered saline (pH 7.35), at 40–50°C for 2–4 hours (Wiser and Callaway, 1996).

Myelin staining

For myelin staining, a modified version of the Gallyas protocol was used (Gallyas, 1979; Hess and Merker, 1983).

Microsphere injections

Animals of PND 10–12 were anesthetized with an intramuscular injection of 90 mg/kg ketamine, 10 mg/kg xylazine solution. Rhodamine-labeled latex microspheres (Lumafluor), 0.02–0.2 μm in diameter, were chosen as retrograde tracers (Katz et al., 1984). The microspheres were pressure-injected through a broken-tip glass electrode in the superior colliculus by using a Picospritzer (General Valve Corporation) based on experimentally de-

termined stereotaxic coordinates, adjusted to the age of the animals. The skin over the scalp was resealed, and the animals were allowed to recover on a slide warmer set to approximately 35°C. These animals were sacrificed for electrophysiological experiments that included filling the cells with biocytin 2–4 days after the injections were made.

Golgi staining

We used a modified version of the rapid Golgi method (Strausfeld, 1980). After fixation, samples were incubated in a chromating solution of 2% potassium dichromate and 5% glutaraldehyde for approximately 36 hours. Metal impregnation was then done in 0.75% silver nitrate solution for 24–36 hours. After the first round of staining, brains were divided into two hemispheres and the chromation and silver impregnation steps were repeated. All incubations were done in the dark at RT. Finally, hemispheres were dehydrated in increasing concentrations of EtOH, immediately embedded in paraffin at 37°C, and sectioned at 100 μm on a sliding Vibratome (AO Instrument Co.). Sections were mounted on clean slides and cover-slipped in Permount (Fisher).

Intracellular injections with biocytin

For biocytin staining, cells were injected intracellularly through a patch pipette containing 0.1%–0.3% biocytin (Molecular Probes). At the end of the experiment, the slices were fixed in 4% paraformaldehyde in 0.1 M PB (pH 7.4) at least overnight at 4°C. The slices were processed with the ABC Elite kit (Vector Laboratories), and the biocytin-injected cells were revealed with diaminobenzidine (DAB; Sigma) and Ni^{+} in nickel ammonium sulfate as the chromogen. Cortical layers were identified by differential interference contrast (DIC) microscopy or by counterstaining the sections with Nuclear Yellow (Molecular Probes).

DiOlistics

We followed the protocol of Gan et al. (2000), with minor modifications. The cartridges required for the gene gun were made with the Tubing Prep Station provided by Bio-Rad. A total of 1.5 mg of dye was diluted in 50 μl of methylene chloride, and 12.5-mg tungsten or gold (1.0–1.7 μm diameter) microcarriers were placed on a clean glass slide. The dye solution was poured on the particles and allowed to dry. The dye-covered particles were scraped off the slide, dispersed in 3 ml of ddH_2O, and placed in a sonicator for approximately 20 minutes. The solution was then placed in the tubing that was rotated for 15 minutes so that the inner surface would be covered by the particles. The water was then slowly removed and dried with a low nitrogen flow. The tubing was eventually cut and used as cartridges. For the actual delivery of the particles on slices, the gene gun was attached to a helium tank. The gas pressure was set to 120–150 psi, and the device was placed approximately 1 cm above the slice. Each slice was "shot" once. After an approximately 30-minute incubation in the ACSF at RT to allow for the dye to diffuse, the slices were fixed in 4% paraformaldehyde. After this point, sections were stored at 4°C in the dark. After a minimum of 3 hours, the sections were rinsed with 0.1 M PB and cover-slipped with Vectashield (Vector Laboratories). DiI-labeled cells were visualized on a custom made two-photon scanning microscope (Majewska et al., 2000) with 800-nm excitation. Images were acquired by using Fluoview software (Olympus). Optical sections were taken 1 μm apart, and the image stacks were imported into Neurolucida (MicroBrightField, Inc.) to obtain 3-D reconstructions of the imaged cells.

Reconstructions and measurements

Cells were reconstructed three dimensionally with the Neurolucida workstation. Biocytin-stained and silver-impregnated cells were visualized with transmitted light under DIC optics on an Olympus inverted microscope. Most cells were drawn with a 60×, 0.90 NA water-immersion objective. The reconstruction of fluorescently labeled cells was done from the acquired stacks of images. The measurements of the morphologic variables were also done with Neurolucida.

Statistical analysis

Principal component analysis (PCA). We used PCA to select variables that contributed most to the overall variability and, thus, were more important in distinguishing different morphologic cell classes. We then used these variables for the cluster analysis that resulted in the actual classification scheme.

PCA is a data-reduction method. It transforms the original data set into a set with fewer variables (components). These components are sorted in descending order of their contribution to the overall variance. The argument for its usefulness is that variables that account for most of the overall variability should better reflect differences among different cell types. The goal is to replace the original data set (seen as a matrix) by another matrix with fewer variables (or dimensions) while preserving as much of the original information as possible (Marcoulides and Hershberger, 1997). This strategy would make the ratio of number of cases to the number of variables larger and, therefore, make the cluster analysis more stable.

Measurements for each variable in our data set were transformed to standard scores across all cells based on the commonly used formula $(x_i - \text{mean})/s$. Standardization leads to unit-less values, thus removing any arbitrary effects due to the choice of variable units. In addition, by conforming all variables to the same range of values, all are weighted equally (Romesburg, 1984). In the correlation matrix, certain variables were highly correlated ($r > 0.8$) with each other, for example, somatic area and somatic perimeter. This practically meant that these variables reflected similar features of the cells. To avoid artificially weighting these variables (or features) in the cluster analysis, one of the two was excluded. Of the pairs of highly correlated variables, the one with the lower value in the principal component loadings table was removed.

Data reduction in PCA was achieved by selecting a subset of principal components based on the Kaiser criterion (Kaiser, 1960) and scree plot (Cattell, 1966), according to which, selected principal components have an eigenvalue greater than or equal to 1. The scree plot is a graph of the eigenvalues versus their ordinal value. An acceptable threshold is set where this graph plateaus: factors beyond that threshold do not add significantly to the overall variance and, therefore, can be excluded.

Cluster analysis. The term cluster analysis refers to mathematical methods that group objects (cases) of a data set based on their degree of similarity. All cases are first

plotted in a multidimensional space. A certain measure of proximity is chosen, and clusters are eventually formed by the cases that fulfill the criteria of the clustering method selected. Our analysis was performed with Euclidean distances by using Ward's method. According to Ward's method, cases are assigned to clusters so that the variance (sum of squared deviations from the mean) within each cluster is minimized. This method resulted in well-defined groups in this study.

For the purpose of describing the final classification scheme in an accessible way, we report P values from two-tailed t tests among variables that define the different cell classes. These statistical comparisons were performed with the statistic toolbox of Excel (Microsoft). Principal component analysis and cluster analyses were performed with the Statistica software package (StatSoft, Inc.).

RESULTS

Identification of mouse primary visual cortex and cell labeling

Our goal was to sample layer 5 of mouse primary visual cortex, a relatively small region of the cerebral cortex, to arrive at a relatively complete anatomic classification of the neurons. In these experiments, the primary visual cortex was defined in coronal sections by using different histologic methods. In sections processed with cresyl violet, the primary visual cortex was characterized by the darker staining of layer 4 due to the higher density of small cells (Fig. 1A). A similar pattern was seen with cytochrome oxidase staining (Fig. 1B). Finally, we used myelin staining (Fig. 1C), because the medial border of the primary visual cortex can be detected by myelin fibers extending perpendicularly to the cortical layers reaching layers 2/3, as well as by two myelin plexi extending horizontally in layers 4 and 5.

Layer 5 was also identified by its unique population of large pyramidal cells. The border with layer 4 was usually easily detected due to increase in cell density in layer 4, whereas the border between layer 5 and 6 was less clear, although a decrease in the number of large pyramidal neurons was always detected in more inferior positions.

We labeled and reconstructed 158 neurons by using three different staining procedures (Fig. 2). To achieve a relatively unbiased sampling of the morphologies of neurons present, most of the cells were stained using DiOlistics (Fig. 2C; n = 100). We also reconstructed a population of 53 pyramidal neurons that had been recorded with whole-cell electrodes and filled with biocytin (Fig. 2B). Finally, we reconstructed five cells impregnated by using a modified version of the rapid Golgi method (Strausfeld, 1980; Fig. 2A).

To identify a morphologically and physiologically homogeneous class of cells, we also reconstructed 27 pyramidal cells that project to the superior colliculus. These biocytin-filled neurons, which are considered relatively homogeneous in terms of morphology and physiology, also served as an additional marker of primary visual cortex and were indeed remarkably similar to each other, in agreement with previous studies (Schofield et al., 1987; Hallman et al., 1988; Kozloski et al., 2001). This group was used as a control for the classification analysis described below.

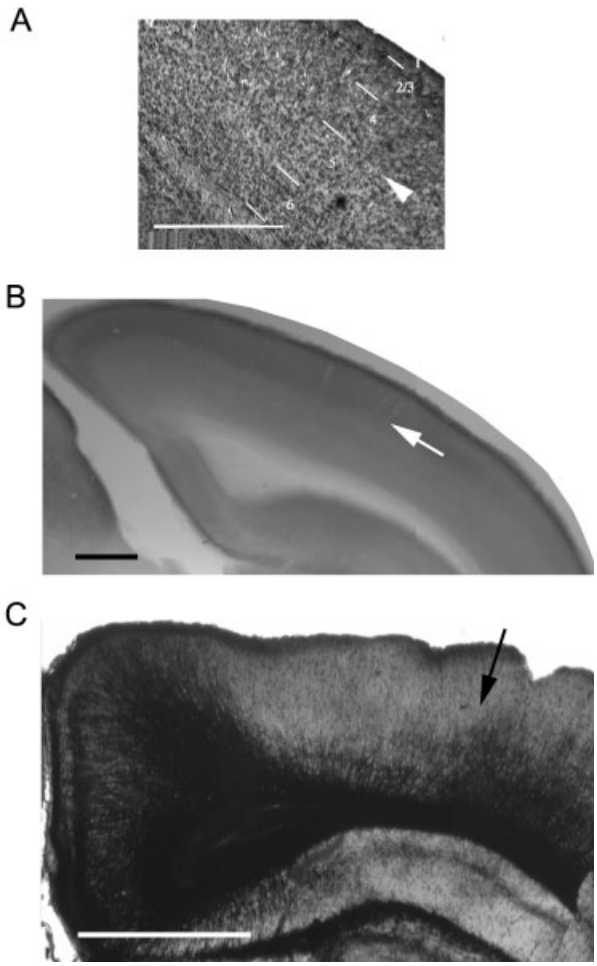

Fig. 1. Identification of the mouse primary visual cortex. Coronal sections through the posterior pole of the cerebral hemisphere. **A:** Nissl stain. Note the prominent layer 4 due to the high density of small granule cells. Arrowhead points to the distinct border between layers 4 and 5. **B:** Cytochrome oxidase staining. Arrow points to the intense staining near layer 4. **C:** Myelin stain. Arrow points to the medial border of V1. Scale bars = 100 μm in A; 500 μm in B,C.

Morphologic classification: principal component analysis results

With the sample of 158 neurons, we performed a quantitative morphologic classification by using principal component analysis and cluster analysis. We first measured, for each neuron, the following 33 morphologic variables: (1) Somatic area. The soma was reconstructed as a 2-D contour at the plane of sharpest focus. Thus, all somatic measurements refer to an XY projection. (2) Somatic perimeter. (3) Number of primary dendrites, i.e., dendrites that stem directly from the soma. (4) Somatic axes ratio, i.e., the ratio of the somatic axis along the direction of the cell (vectorial average of the circular distribution of dendrites) to the longest perpendicular axis. This variable reflects how elongated the soma is. (5) Base-10 logarithm of the somatic axes ratio, as a way to better distinguish between vertically and horizontally elongated somata. (6) Somatic aspect ratio, defined as the ratio of the longest

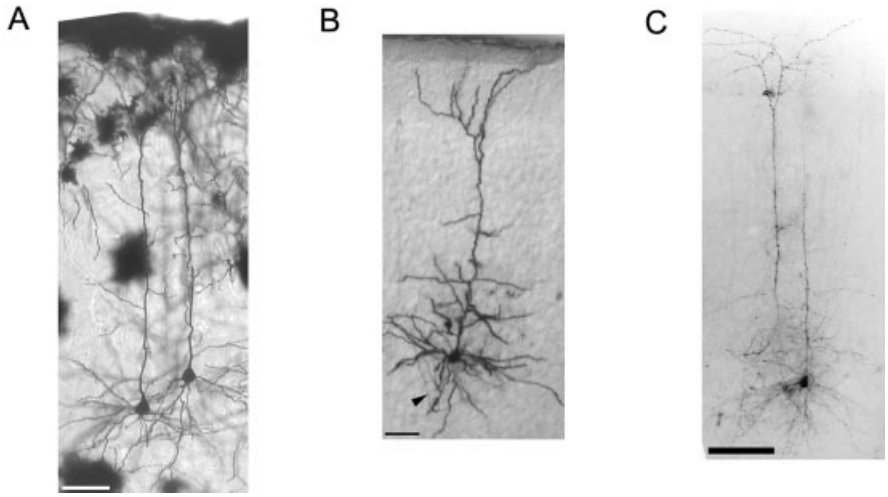

Fig. 2. Methods for labeling individual cortical cells. **A:** Golgi method. Multiple neurons in a single slice are stained with this silver impregnation technique. **B:** A pyramidal cell in a coronal section from mouse visual cortex injected intracellularly with biocytin and then processed for visualization. Intracellular biocytin staining allows a fairly accurate reconstruction of the dendritic arbor of the neuron. Structures as small as spines (~1 μm in diameter) can be visualized. Arrowhead points to the axon. **C:** Cells labeled with the DiOlistics method. DiOlistically labeled neurons were imaged on a two-photon scanning microscope, and the morphology was reconstructed. The image is a projection of a series of images acquired in the z-axis. Spines can also be visualized. Scale bars = 100 μm in A,C, 50 μm in B.

axis of the soma to the shortest perpendicular axis. (7) Somatic circularity index = $(4 \times \pi \times \text{area})/(\text{perimeter})^2$. Values closer to one represent more circular somata. (8) Somatic compactness = $(\sqrt{(4 \times \text{area})}/\sqrt{\pi}) \times$ max axis, where max axis is the longest somatic axis. Values further from one represent less compact somata. (9) Somatic roundness = $(4 \times \text{area})/\pi) \times (\text{max axis})^2$. The closer to one this value is, the more circular the soma. This measure is similar to the circularity index; however, it helps to detect minute differences in cell contour; for example, roundness helps to distinguish pyramidal/conical somata from round or triangular ones, whereas the circularity index distinguishes circular or oval-shaped somata from irregularly shaped ones. (10) Total basal length, i.e., the sum of the length of the basal dendrites. Basal dendrites are defined as the primary dendrites stemming from the cell bodies of pyramidal neurons, except for the apical dendrite, which is defined as a thicker dendritic process that clearly emanates from the apical part of the soma and extends toward the upper cortical layers. (11) Number of primary basal dendrites. (12) Average length of the primary basal dendrites. (13) Average tortuosity of the basal dendrites. Tortuosity is defined as the branch length (distance along the path of the branch) divided by its radial (straight line) length. (14) Total 3-D tile area, where the total tile is the 3-D contour created by connecting the ends of all dendrites with straight lines. The area is calculated from the tile's XY projection. (15) Total 3-D tile perimeter. (16) Total 3-D tile circularity index. (17) Total 3-D tile aspect ratio, which is the ratio of maximum to the minimum diameter of the tile. (18) Base-10 logarithm of the total 3-D tile aspect ratio. (19) Total 3-D tile depth, defined as the distance between the furthest points of the tile in the z axis (horizontal plane of the tissue). (20) Basal 3-D tile depth, where basal tile is the 3-D contour created by connecting the ends of the basal dendrites (when defined) with straight lines. (21) Total 2-D tile perimeter, which is the perimeter of the tile projected onto the XY (frontal/coronal) plane. (22) Distance to apical bifurcation (base of the tuft) measured from the base of the apical dendrite. (23) Number of apical dendrite branches. (24) Average length of apical branches. (25) Total length of the apical tuft, which is the sum of the lengths of the branches that form the tuft. (26) Length of the horizontal axis of the apical tuft, defined as the distance from one end of the tuft to the most distal edge on the mediolateral axis. (27) Length of the vertical axis of the apical tuft, defined as the distance from the base of the tuft to the most distal edge on the dorsoventral axis. (28) Apical tuft axes ratio, defined as the ratio of the horizontal to vertical axis of the apical tuft. (29) Thickness of the apical dendrite at approximately 60 μm from the soma. (30) Total length of all dendrites. (31) Average dendritic length, defined as the average length of each primary dendrite. (32) Average dendritic tortuosity. (33) Maximum dendritic length, i.e., length of the longest primary dendrite.

A matrix of cell morphology measurements was then created, where each cell was represented by 33 numbers, analogous to a vector in a 33-dimensional space. After removing the redundant morphologic variables as described in the Materials and Methods section, 21 variables were selected for PCA. The results of the PCA are shown in Table 1. The first five principal components had eigenvalues greater than 1 and accounted for 70% of the total variance. The scree plot flattened beyond the fifth component. A total of 14 variables (labeled in bold and italics in Table 1) that showed significant loadings (absolute value ≥ 0.7) were eventually selected for the cluster analysis.

Cluster analysis classification

We then performed cluster analysis by using the 14 selected variables and classified the 158 neurons into two major classes (named class 1 vs. 2–5), including several subgroups (named 1A, 1B, 2A, etc.). The corresponding dendrogram is shown in Figure 3, where every point on

TABLE 1. Principal Component (PC) Loadings of the 21 Variables Included in PCA[1]

	PC 1	PC 2	PC 3	PC 4	PC 5	PC 6	PC 7	PC 8	PC 9
#1-soma area	0.53	−0.03	−0.22	−0.25	−0.01	0.56	−0.01	−0.29	0.07
#3-# 1o dendrites	0.22	−0.23	−0.13	−0.07	***0.88***	−0.11	−0.14	−0.02	0.00
#4-soma axes ratio	0.00	0.32	−0.68	0.10	−0.10	−0.08	−0.09	−0.44	0.34
#7-soma circularity	0.13	−0.31	***0.74***	−0.14	−0.11	0.02	0.08	−0.33	0.24
#9-soma roundness	0.08	−0.39	***0.81***	−0.17	0.00	−0.02	0.06	−0.06	0.09
#14-3-D total tile area	***0.81***	0.08	−0.14	−0.28	−0.07	0.09	0.19	0.06	−0.11
#16-3-D total tile circularity	−0.15	***0.86***	0.40	−0.04	0.14	−0.03	−0.05	−0.18	−0.15
#17-3-D total tile aspect ratio	−0.13	***0.86***	0.40	−0.05	0.14	−0.05	−0.03	−0.17	−0.15
#19-total tile depth	−0.20	0.60	0.12	0.09	−0.04	0.19	0.12	0.46	0.41
#22-length to apical bifurcation	0.69	0.02	0.03	−0.37	−0.15	−0.30	0.01	0.09	0.00
#23-# apical collaterals	***0.80***	0.07	0.05	0.05	0.11	−0.20	0.03	0.06	0.18
#24-avg apical collateral length	0.46	0.12	−0.19	−0.55	−0.23	−0.27	−0.11	0.06	−0.26
#25-total tuft length	***0.87***	0.05	0.10	0.32	0.07	−0.01	0.10	−0.01	0.03
#26-horizontal tuft axis	***0.85***	0.04	0.12	0.24	0.01	0.27	−0.17	0.08	−0.01
#27-vertical tuft axis	***0.75***	0.08	0.00	0.07	0.07	0.05	0.18	0.11	0.01
#28-horiz : vertical tuft axes ratio	0.62	−0.05	0.18	0.26	−0.12	0.32	−0.52	0.07	−0.22
#29-apical thickness	0.56	0.09	0.07	−0.31	−0.08	−0.19	−0.50	0.08	0.36
#30-total dendritc length	***0.92***	0.02	−0.06	0.03	0.24	−0.07	0.12	−0.07	−0.02
#31-avg dendritic length	***0.85***	0.11	−0.05	0.04	−0.26	0.05	0.22	−0.11	−0.07
#32-avg dendritic tortuosity	0.20	−0.08	0.09	***0.70***	−0.24	−0.42	−0.09	−0.10	−0.06
#33-max dendritic length	***0.93***	0.07	0.00	0.15	0.10	−0.09	0.15	−0.01	0.05
Eigenvalue (variance)	7.62	2.30	2.20	1.50	1.15	0.98	0.79	0.74	0.70
Proportion of total	0.36	0.11	0.10	0.07	0.05	0.05	0.04	0.04	0.03

[1]Each column in the table corresponds to a principal component. Principle components are arranged in order of decreasing eigenvalue. Variables with absolute loading values > 0.7 that were included in the cluster analysis are noted in bold and italics. The absolute loading values ≥ 0.7 are also noted in bold and italic.

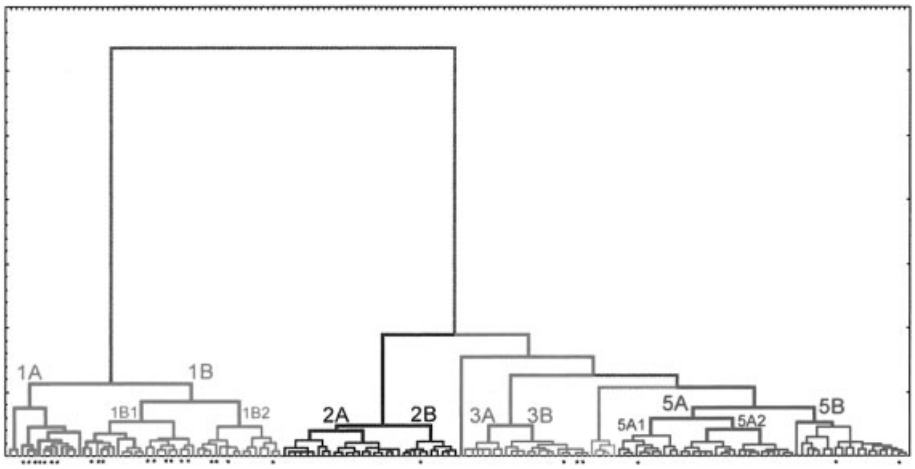

Fig. 3. Cluster analysis. Dendrogram for 158 cases after principal component analysis. Each point on the x-axis corresponds to a cell. Asterisks indicate corticotectal neurons. The linkage distance is plotted in arbitrary units on the y axis, reflecting the degree of dissimilarity between cases or groups. Five groups and several subgroups within each can be distinguished. [Color figure can be viewed in the online issue, which is available at www.interscience.wiley.com]

the x-axis represents a cell. The linkage distance is plotted on the y axis. The asterisks indicate cells that have been microsphere labeled from the superior colliculus injections, i.e., corticotectal (CT) cells.

Class 1: tall pyramidal neurons

Common features of group 1. The first main left branch of the dendrogram (Fig. 3) included "typical" large pyramidal neurons, which are arguably the distinguishing feature of layer 5 throughout the neocortex, because pyramidal neurons in other cortical layers are smaller. These cells (Fig. 4) had significantly larger conical cell bodies (mean area of largest cross-section: 213.4 $\mu m^2 \pm 71.7$, n = 48, for group 1 vs. 153.9 $\mu m^2 \pm 77.3$, n = 110, for groups 2–5, $P << 0.001$). Another distinguishing feature was a relatively thick apical dendrite (1.9 $\mu m \pm 0.6$ at approximately 60 μm distally from the soma) that extended perpendicularly through the cortical layers reaching layer 1, where it branched out to form the apical tuft. The apical tuft extended in the horizontal plane and was usually restricted between layer 2 and the pia mater. The elaborate and extensive apical tuft appeared to be the key variable that distinguished the first major group of cells from the rest of the cases. This feature was reflected by the larger total tile area measurements (62,037.0 $\mu m^2 \pm$ 25,572.8 for group 1 vs. 24,600.1 $\mu m^2 \pm$ 19,313.8 for groups 2–5; $P < 0.001$) and the lower total tile circularity index measurements compared with all the other cells (0.12 ± 0.06 for group 1 vs. 0.24 ± 0.13 for groups 2–5; $P < 0.0001$). All other primary dendrites emanated from the soma in different directions, forming the basal dendritic arbor of various shapes and sizes. Overall, the dendritic tree of these cells was symmetric along the dorsoventral axis in the coronal plane. The dendrites of the cells in this group had spines, with the exception of two cells that

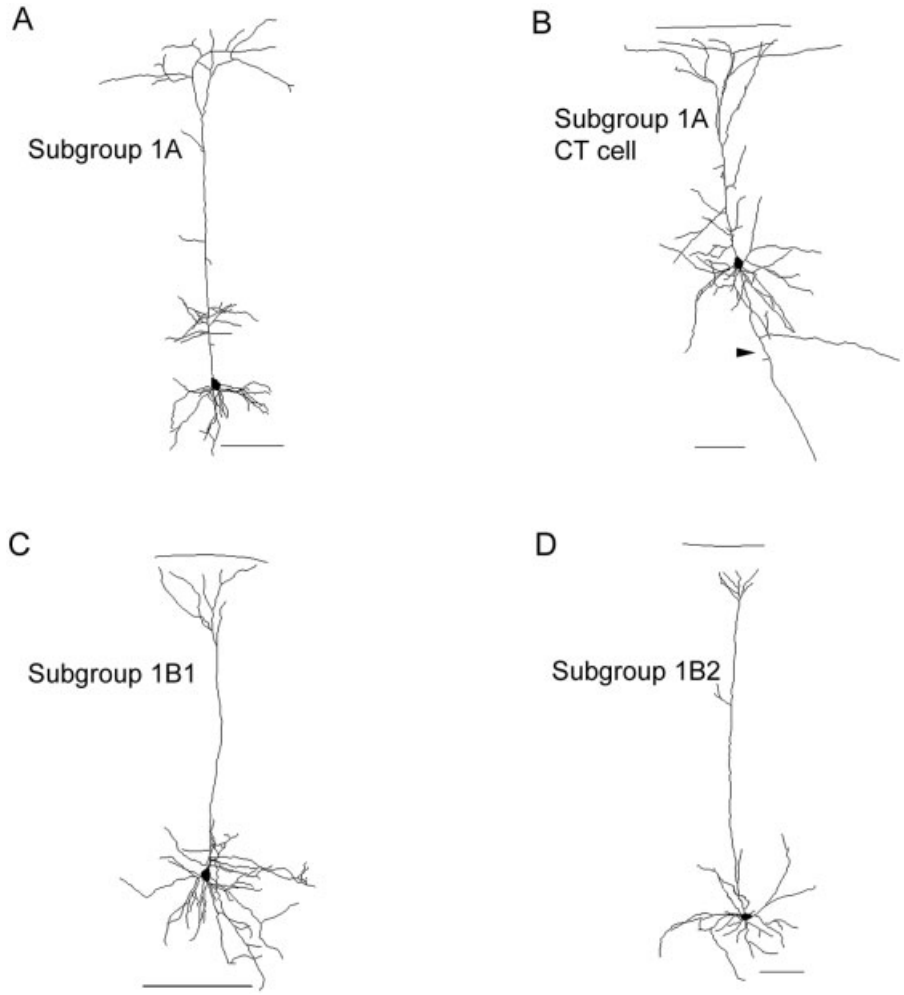

Fig. 4. Group 1. Examples of cells of group 1. Tall pyramidal neurons. **A,B:** Examples of subgroup 1A characterized by extensive apical tufts. The cell in B is a corticotectal cell. Arrowhead points to the axon. **C:** Example of subgroup 1B1, which includes tall pyramidal cells with narrow apical tufts and elongated cell bodies. **D:** Example of subgroup 1B2, which includes tall pyramidal cells with narrow apical tufts and round cell bodies. Cells are oriented so that the pia mater is at the top and horizontal and medial is to the left. Scale bars = 100 μm in A–D.

appeared to be aspiny, possibly due to incomplete biocytin staining.

Subgroups of group 1. Within group 1, two subgroups were distinguished: tall wide-tufted pyramidal neurons (labeled 1A on the dendrogram; Fig. 4A,B) and tall narrow-tufted pyramids (labeled 1B; Fig. 4C,D). Subgroup 1A had larger somata on average (somatic area, 261.3 ± 68.2 μm^2, n = 13, for group 1A vs. 195.6 3 ± 65.3 μm^2, n = 35, for group 1B; $P < 0.05$), but its more distinctive feature was the more extensive dendritic tree. Although the number (11.1 ± 3.5 vs. 9.8 ± 4.5; $P > 0.1$) and length (108.8 μm ± 26.6 vs. 107.1 μm ± 38.7; $P > 0.5$) of the apical branches was similar between the two subgroups, the apical tufts were not. In the first group (1A), the apical tuft extended further horizontally (horizontal axis, 300.6 μm ± 104.4 vs. 181.1 μm ± 86.2; $P < 0.01$) and the initial branching point was more distal (vertical axis, 202.0 μm ± 112.5 vs. 105.6 μm ± 46.4; $P = 0.01$); in the second group, the tufts were narrower and more restricted to the upper cortical layers. The ratio of the tuft axes was the same (2.0 ± 1.2 vs. 1.9 ± 1.2; $P = 0.93$), but the total length of the apical tuft was higher for the first subgroup (1,849.7 μm ± 914.9 vs. 847.3 μm ± 433.0; $P < 0.01$). The most extreme cases that made this point very clear were the two neurons in this group whose apical dendrites bifurcated at approximately the midpoint of the apical dendrite, in layer 3. In terms of the basal dendritic arbors, the total length was similar (1,698.6 μm ± 514.5 vs. 1537.4 μm ± 818.5; $P > 0.1$), but on average class 1A neurons had fewer (5.8 ± 2.0 vs. 7.4 ± 2.5; $P < 0.05$) and longer (313.9 μm ± 114.1 vs. 208.8 μm ± 83.2; $P < 0.01$) primary basal dendrites. As a result, the basal arbors of subgroup 1A were more compact in most cases, i.e., they could be enclosed by a circle centered at the cell body, as opposed to 1B where that part of the dendritic tree is skewed.

The tall narrow-tufted pyramids of subgroup 1B could be further subdivided into two subgroups: one with elongated cell bodies (1B1; Fig. 4C) and another with round cell bodies (1B2; Fig. 4D). The latter subgroup was characterized by cells having slightly smaller somata (200.2

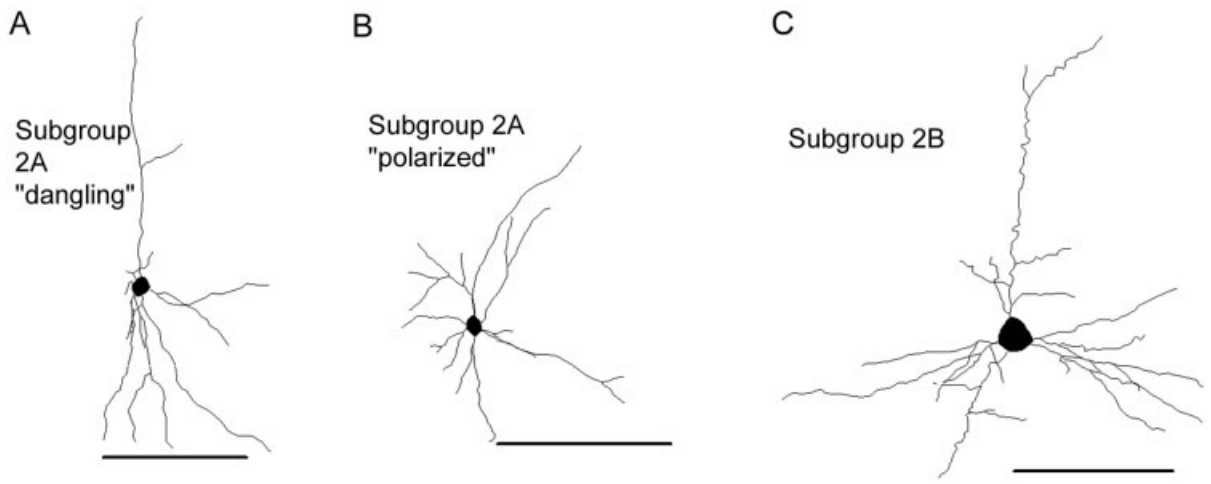

Fig. 5. Group 2. Examples of cells of group 2. Cells with polarized dendritic arbors (mostly multipolar) and short pyramidal neurons. **A:** Example of subgroup 2A. Case of a "dangling" pyramidal cell. Note basal dendrites extending in a limited region opposite to the apical dendrite, terminating in layer 6. **B:** Example of subgroup 2A. Note the "polarized" dendritic arbor. The dendrites branch only within a certain area around the cell body. **C:** Example of subgroup 2B. A "short" pyramidal neuron. The apical dendrite ends at approximately 100 μm from the cell body. Cells are oriented so that the pia mater is at the top and horizontal and medial is to the left. Scale bars = 100 μm in A–C.

$\mu m^2 \pm 62.6$, n = 20, for subgroup 1B1 vs. 189.5 $\mu m^2 \pm$ 70.5, n = 15, for subgroup 1B2; $P > 0.5$), which were less elongated, resulting in an equilateral triangular projection in the transverse plane. This finding is quantitatively reflected by the somatic axes ratio (1.5 ± 0.3 for 1B1 vs. 1.2 ± 0.3 for 1B2; $P < 0.01$), roundness (0.6 ± 0.09 for 1B1 vs. 0.7 ± 0.08 for 1B2; $P < 0.001$), and circularity index (0.8 ± 0.07 for 1B1 vs. 0.9 ± 0.04 for 1B2; $P < 0.001$) measurements. Features related to the apical and basal dendrites were similar between these two subgroups.

Class 2: short pyramidal and large multipolar cells

Common features of group 2. This group was characterized by neurons without apical tufts and short pyramidal or multipolar morphologies (Fig. 5). With the exception of group 4, which was composed of very small cells that will be described below, all groups of cells in the right main branch of the dendrogram, i.e., groups 2, 3, and 5, had similarly sized cell bodies with an average somatic area of 153.9 $\mu m^2 \pm 79.3$. There was no significant difference is cell body size between group 2 and groups 3 and 5 (mean somatic area 146.3 $\mu m^2 \pm 65.1$, n = 31, for group 2 vs. 163.2 $\mu m^2 \pm 80.4$, n = 74, for groups 3 and 5; $P > 0.1$). However, the somata of group 2 tended to be rounder and more compact than all the other cases, as reflected by measurements of somatic axes ratio (1.26 ± 022, n = 31, for group 2 vs. 1.54 ± 0.34, n = 79, for groups 3–5; $P < 0.001$) and somatic roundness (0.71 ± 0.08 vs. 0.55 ± 0.09; $P < 0.001$). Perhaps the most striking common feature among group 2 cells was the lack of an apical tuft; cells either did not have an apical dendrite or, if one was present, it did not form a tuft at its distal end.

Subgroups of group 2. This class can be subdivided into two subgroups, labeled 2A (polarized multipolar cells; Fig. 5A,B) and 2B (short pyramidal neurons; Fig. 5C). There are no significant differences in size and shape of the cell bodies: mean somatic area for 2A was 130.4 $\mu m^2 \pm$ 50.5, n = 21, vs. 179.5 $\mu m^2 \pm 81.7$, n = 10, $P = 0.1$; mean somatic roundness 0.69 ± 0.08 for 2A vs. 0.75 ± 0.08 for 2B, $P > 0.05$. The distinguishing feature between these subgroups was the extent and overall shape of the dendritic arbor. This finding is because, although the average number of primary dendrites was the same (6.4 ± 2.0 for 2A vs. 6.0 ± 1.7 for 2B; $P > 0.5$), the average primary dendritic length was different (126.4 μm ± 54.8 for 2A vs. 288.6 μm ± 80.5 for 2B; $P = 0.0001$). In addition, on average, cells of group 2B had a higher maximum dendritic length (267.2 μm ± 122.4 for 2A vs. 793.8 μm ± 269.7 for 2B; $P = 0.0001$), which was the tuft-less apical dendrite mentioned above. Moreover, these general differences in dendritic trees were reflected by the tile measurements. Cells of group 2A had significantly less extensive dendritic trees (total tile area, 9,808.4 $\mu m^2 \pm$ 6,141.0 for 2A vs. 23,515.6 $\mu m^2 \pm$ 11,856.9 for 2B; $P < 0.01$) that could be confined within a more circular enclosure around the cell, as reflected by a higher total tile circularity index (0.32 ± 0.15 for 2A vs. 0.17 ± 0.08 for 2B; $P < 0.01$). Indeed, the average total tile circularity index of neurons in 2B was close to that of the tall pyramidal neurons of group 1. This fact and the presence of a relatively small, yet distinct, apical dendrite, form the basis of our characterization of the 2B cells as short pyramidal neurons. These short apical dendrites usually terminated in layer 3, approximately 150 μm from the soma, were thinner than their counterpart tall pyramidal neurons (average apical dendrite thickness, 1.63 μm ± 0.52 for 2B vs. 1.93 μm ± 0.64 for group 1; $P > 0.1$), and gave rise to fewer branches (average number of apical branches 6.1 ± 1.7 for 2B vs. 10.2 ± 4.3 for 1; $P < 0.0001$).

Another morphologic variable that distinguished the two subgroups was the degree of symmetry in the dendritic tree. Like the pyramidal cells of group 1, the short pyramidal neurons were symmetric with respect to the dorsoventral axis in the coronal plane. In contrast, practically all the members of the 2A subgroup had asymmetrical dendritic trees.

In summary, this class of tuft-less neurons included a group of multipolar cells with dendritic arbors that showed a certain orientation or polarity and a group of

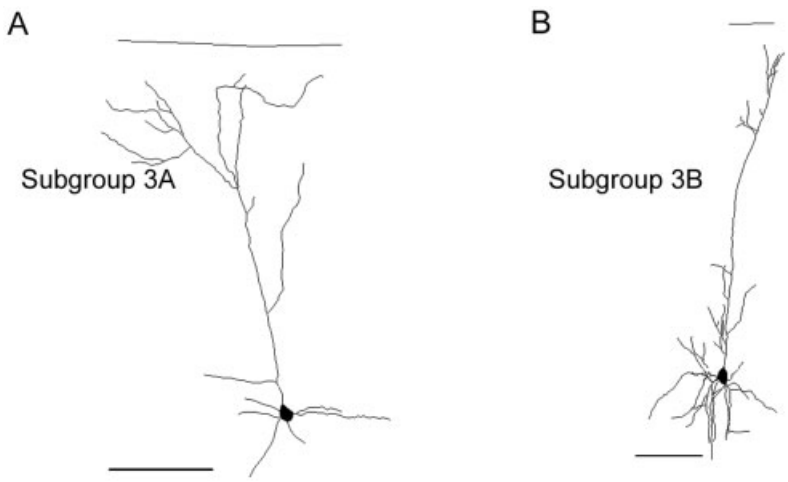

Fig. 6. Group 3. Examples of cells of group 3. Pyramidal cells with small dendritic arbors. These cells have conical somata. The dendritic arbors are less extensive than those of the large pyramidal neurons, especially when comparing the apical dendrites. **A:** Example of subgroup 3A. "Diffuse" dendritic arbors. **B:** Example of subgroup 3B. Note the overall narrow dendritic field. Cells are oriented so that the pia mater is at the top and horizontal and medial is to the left. Scale bars = 100 μm in A,B.

short pyramidal neurons. We do not think that the latter are the result of an artifact, due to incomplete staining or sectioning, because these short apical dendrites taper off at the distal end, instead of forming a bleb of any sort which would have been an indication of artificial physical damage to the tissue.

Class 3: narrow pyramidal neurons

Common features of group 3. For the most part, this group included neurons with conical cell bodies, as well as distinct basal and apical regions, and as such could be characterized as pyramidal (Fig. 6). Even though the size of the cell bodies did not vary significantly, the somatic shape was more similar to that of the tall pyramidal neurons included in the first main branch (group 1; for example, somatic roundness, 0.63 ± 0.11 for group 1 vs. 0.59 ± 0.07 for group 3, n = 23; $P > 0.01$) rather to the short pyramidal cells described in group 2 (somatic roundness, 0.71 ± 0.08 for group 2 vs. group 3; $P < 0.0001$). Nevertheless, the extensive and elaborate apical tufts seen in group 1 were not encountered in group 3. In this case, the apical dendrites reached the upper cortical layers, but the tuft was relatively small (total tuft length, 416.2 μm ± 362.8, n = 23, for group 3 vs. 1,136.9 μm ± 756.0 for group 1; $P < 0.0001$) having a narrow horizontal extent (horizontal axis of the tuft, 112.0 μm ± 104.0 for group 3 vs. 215.7 μm ± 105.8 for group 1; $P < 0.01$). The apical dendrites gave rise to fewer branches (3.9 ± 3.4 for group 3 vs. 10.2 ± 4.3 for group 1; $P < 0.001$) that were of similar length.

Subgroups of group 3. We could distinguish two subgroups: one of "diffuse" dendritic arbors (subgroup 3A) and one of "narrow" pyramidal neurons (subgroup 3B). These groups were mainly distinguished from each other by their apical tuft. The most striking feature of the cells in group 3B was the narrow apical tuft, which consisted only of a few branches at the distal end of the apical dendrite, which barely reached layer 1. In the cells of 3A, the initial branching point for the tuft was approximately at the same level as in 3B (vertical axis of tuft, 127.7 μm ± 78.1 for 3A, n = 8, vs. 74.0 μm ± 50.8 for 3B, n = 9; $P > 0.1$), but its branches were not confined in such a narrow region (horizontal axis, 186.9 μm ± 105.0 for 3A vs. 45.5 μm ± 37.0 for 3B; $P < 0.01$). Another feature that stood out in these cases was the symmetry of the dendritic trees, although there was a small degree of overlap between the two subgroups in this respect: most of the cells in 3B were symmetrical with respect to the dorsoventral axis, especially in the basal region, whereas the dendritic arbors of cells in 3A showed some degree of directionality, branching out to a higher degree in a certain region around the cell body.

Subgroup 3A also included three cells that were not obviously pyramidal. The reason they were included in this group by the algorithm is most probably the somatic characteristics. In addition, two of the three had a thicker dendrite branching off the apical part of the soma, which in quantitative terms could be interpreted as an apical dendrite because they possess similar features. Subgroup 3B includes a few cases of pyramidal neurons with apical dendrites terminating 100–200 μm from the soma.

Class 4: small cells

Group 4 comprised the smallest cells of our data set, in terms of both somatic and dendritic characteristics (Fig. 7). The somata of these cells were significantly smaller compared with all the others of the second main group of our classification scheme (somatic area, 64.0 μm^2 ± 28.8, n = 5, for group 4 vs. 158.2 μm^2 ± 76.3, n = 105, for group 2, 3, and 5; $P < 0.001$). In terms of shape, cells of both groups 4 and 5 had significantly more elongated cell bodies, as reflected quantitatively by higher somatic axes ratio measurements (1.56 ± 0.33, n = 56, for groups 4 and 5 vs. 1.35 ± 0.30 for groups 2 and 3, n = 54; $P > 0.001$) and by lower roundness values (0.53 ± 0.09 for groups 4 and 5 vs. 0.66 ± 0.10 for groups 2 and 3; $P < 0.0001$). There was no significant difference between groups 4 and 5 with respect to these variables. The cell bodies were oriented in different directions in the transverse plane.

The dendritic trees of group 4 cells were not very extensive, and this was clearly shown in the tile measurements: total tile area is 5,032.2 μm^2 ± 4,254.8 for group 4 vs.

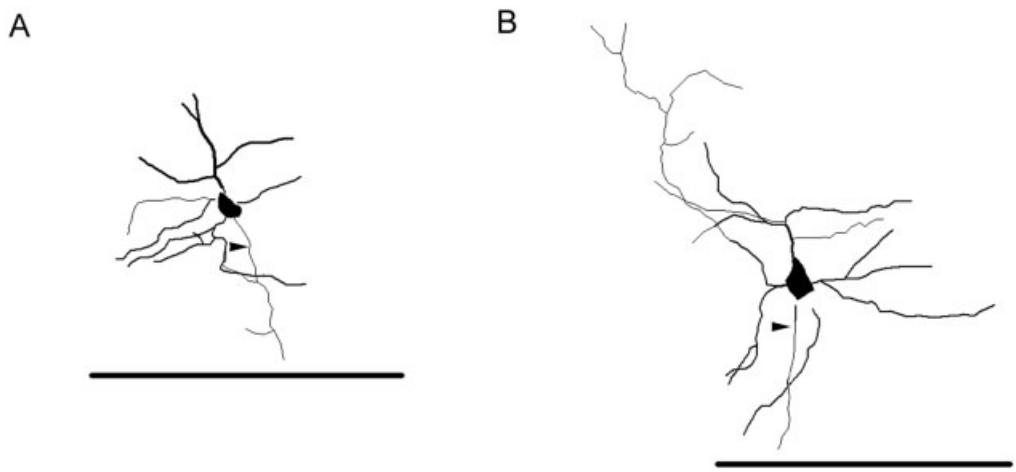

Fig. 7. Group 4. Examples of cells of group 4. Note the small size of the somata and dendritic arbors. Cells are oriented so that the pia mater is at the top and medial is to the left. Arrowheads point to the axons. Scale bars = 100 μm in A,B.

25,640.9 $\mu m^2 \pm$ 19,251.4 for groups 2, 3, and 5; $P <$ 0.0001. The measurements for tile circularity (0.28 ± 0.09 for group 4 vs. 0.24 ± 0.14 for groups 2, 3, and 5; $P > 0.1$) and tile aspect ratio (1.67 ± 0.29 for group 4 vs. 1.97 ± 0.71 for groups 2, 3, and 5; $P > 0.01$) indicated that the dendritic trees overall were equally elongated, even though there seemed to be some degree of asymmetry and directionality within the group of small cells. In addition, the number of primary dendrites was significantly lower among these small cells (4.6 ± 0.9 for group 4 vs. 6.8 ± 2.2 for groups 2, 3, and 5; $P < 0.01$). However, the average (168.7 μm ± 117.2 vs. 239.3 μm ± 130.3; $P > 0.1$) and total (713.0 μm ± 433.7 vs. 1,509.0 μm ± 695.2; $P > 0.01$) dendritic length did not differ significantly. Also, even in the few cases (two of the five cells) where there was a dendrite of a slightly larger diameter than average stemming from the apical part of the soma, it was not as prominent as the apical dendrites of the larger pyramidal neurons.

Most of the small cells had high dendritic tortuosity. There is a statistically significant difference both when compared with group 1 (dendritic tortuosity, 1.86 ± 0.25 for group 4 vs. 1.29 ± 0.16 for group 1; $P < 0.01$) and to the rest of the second main branch of the dendrogram (1.86 ± 0.25 for group 4 vs. 1.15 ± 0.10 for groups 2, 3, and 5; $P <$ 0.01). In summary, this group of cells had the smallest cell bodies with the least number of dendrites with high tortuosity.

Class 5: short pyramidal and atypically oriented cells

Common features of group 5. Similarly to group 2, the common feature of cells of this group was the lack of an apical tuft, either because an apical dendrite did not exist or, when it did exist, it did not form a tuft at the distal end (Fig. 8). The latter cases refer to the so-called short pyramidal neurons, i.e., cells with conical cell bodies with a distinct apical dendrite that terminated approximately in layer 3. The lack of an apical tuft in these cells was not an artifact of sectioning ,because we could observe the terminal tapering of the apical dendrites. At the same time, two variables distinguished cells of group 5 from those of group 2. First, although the cell bodies of the two groups were of similar sizes (somatic area, 161.7 μm^2 ± 83.0, n = 51, for group 5 vs. 146.3 μm^2 ± 65.1, n = 31, for group 2; $P > 0.1$), the former had more elongated cell bodies as indicated by significantly higher somatic axes ratio measurements (1.55 ± 0.33 for group 5 vs. 1.26 ± 0.22 for group 2; $P < 0.0001$) and smaller somatic roundness values (0.53 ± 0.09 vs. 0.71 ± 0.08; $P < 0.0001$). Second, the dendritic arbors of group 5 were less elaborate and extensive on average than those of groups 2 (total dendritic length, 1,611.4 μm ± 632.1 for group 5 vs. 1,091.5 μm ± 670.9 for group 2; $P < 0.01$, and total tile area, 28,396.5 μm^2 ± 21,361.3 vs. 13,920.5 μm^2 ± 10,276.5, respectively; $P < 0.001$). It should be noted that the high standard deviations for the above two variables may reflect heterogeneity in this group.

Subgroups of group 5. Group 5 could be divided into two groups, labeled 5A (n = 31; Fig. 8A,B) with relatively round cell bodies and 5B (n = 20; Fig. 8D) with more elongated somata. Subgroup 5A could be further subdivided into a class of short pyramidal-like neurons with a high number of dendrites (labeled 5A1, n = 11) and another of multipolar cells (labeled 5A2, n = 20). The cell bodies did not vary much in terms of size between subgroups. However, cells of 5B had more elongated cell bodies compared with those of 5A1. These differences were reflected by measurements of the somatic circularity index (0.79 ± 0.06 for 5A vs. 0.68 ± 0.07 for 5B; $P < 0.0001$) and somatic roundness (0.62 ± 0.06 for 5A1 vs. 0.48 ± 0.10 for 5B; $P = 0.0001$).

Cells that formed the subgroup labeled 5A1 could be characterized as pyramidal, or at least pyramidal-like, based on the presence of a distinct dendrite emanating from the apical part of the soma. The apical dendrite gave rise to several branches and in a few cases bifurcated at 50–100 μm from the cell body. It did not extend more than approximately 200 μm, usually ending in layer 3 or 4. These cells had as many primary dendrites as the tall pyramidal neurons of group 1, which is significantly higher than the rest of the groups in the second main branch of our classification tree. Because this difference

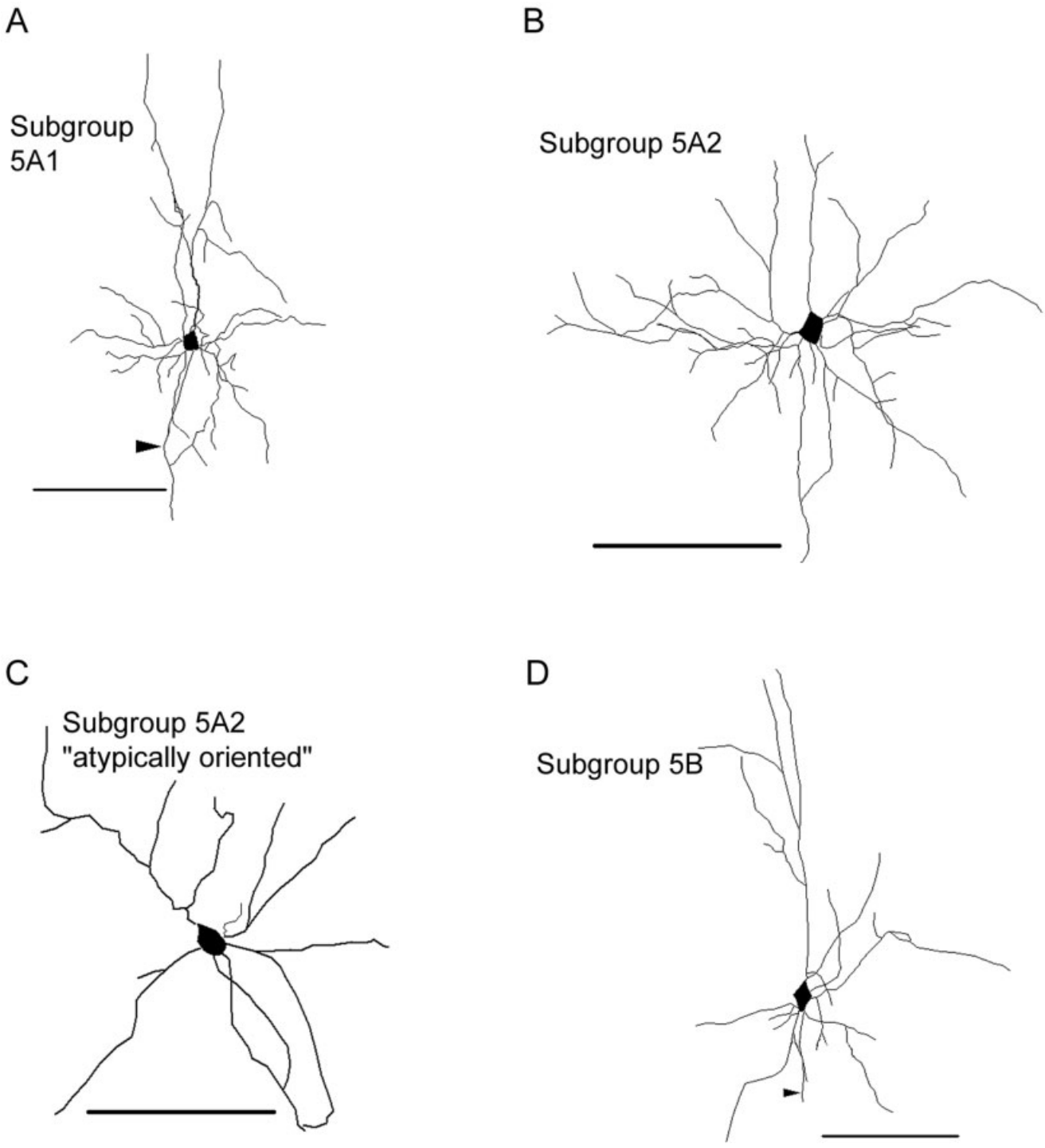

Fig. 8. Group 5. Examples of cells of group 5. This group includes small pyramidal neurons and atypically oriented cells, whose somata and dendritic arbors transverse the cortical layers at an angle other than 90 degrees. **A:** Example of subgroup 5A1. "Short" pyramidal cell with a large number of dendrites. **B:** Example of subgroup 5A2. These cells have fewer primary dendrites on average, compared with subgroup 5A1. Note that the dendritic tree can be enclosed by a circle. **C:** Example of subgroup 5A2. Atypically oriented cell. Note the main axis of the cell crossing diagonally through the cortical layers. **D:** Example of subgroup 5B. A case of a short pyramidal neuron with an elongated cell body. Cells are oriented so that the pia mater is at the top and horizontal and medial is to the left. Arrowheads point to the axons. Scale bars = 100 μm in A–D.

could be statistically significant due to the presence of the small cells of group 4, we repeated the comparison after excluding the group 4 cells and found that the difference remained significant (10.5 ± 2.2 for 5A1 vs. 6.9 ± 2.1 for group 1, 2, 3, 5A2, and 5B; $P < 0.0001$). Although the apical dendrite characteristics of these cells were similar to those of group 2, the larger number of primary dendrites (10.5 ± 2.2 primary dendrites for 5A1 vs. 6.3 ± 1.9 for group 2; $P < 0.0001$), along with the somatic features discussed above, constitute this subgroup a unique class of the so-called short pyramidal cells.

There was a slight difference in the somatic shape between subgroups 5A1 and 5A2 (roundness, 0.62 ± 0.06 for 5A1 vs. 0.53 ± 0.05 for 5A2; $P < 0.01$, although there was no statistical significance in the somatic circularity index), but the variables that distinguished them more clearly were related to dendrites. In addition to the difference in the number of primary dendrites mentioned above, for the latter subgroup, we measured a higher tile circularity index (0.27 ± 0.16 for 5A2 vs. 0.15 ± 0.07 for 5A1; $P < 0.01$), which indicated that the dendritic arbor of these cells can be enclosed by a circular- or oval-shaped outline. This group also included cells that were often atypically oriented, i.e., the cell body and the dendritic tree as a whole extend diagonally, instead of typically perpendicularly, with respect to the cortical layers. Similar cells have been described in rat visual cortex (Miller, 1988).

The cells that made up the last sub-branch of the clustering dendrogram had significantly more elongated somata compared with the members of the neighboring subgroup, as mentioned above. This group included pyramidal neurons with apical dendrites that did not reach layer 1, similar to subgroup 5A1, but had significantly fewer (6.1 ± 2.1 for 5B vs. 10.5 ± 2.4 for 5A1; $P < 0.0001$) and longer (average length, 347.6 μm ± 179.9 for 5B vs. 157.1 μm ± 40.3 for 5A1; $P < 0.001$) primary branches. Finally, the dendritic arbors cover a significantly larger region around the soma (tile area, 40,576.5 μm^2 ± 26,904.0 for 5B vs. 17,718.2 μm^2 ± 7,144.8 for 5A1; $P < 0.01$).

Distribution of the CT neurons in the cluster analysis

We proceeded to examine the cluster analysis classification by analyzing the distribution of CT neurons. Given that information about the projection to the superior colliculus was not included in the cluster analysis, the pattern of the distribution of the CT cells could be used, at least partially, to confirm our classification scheme.

The CT neurons have been described previously in the literature (Schofield et al., 1987). These morphologic descriptions were in agreement with the ones seen in the majority (20 of 27) of CT neurons in group 1. On closer examination, we found one CT cell whose apical tuft was cut in the most distal portion during sectioning or processing of the tissue. The remaining cells of this group were not derived from animals that had been microsphere-injected; therefore, no definitive statement could be made about their identity as CT neurons, although the absence of any retrograde labeling does not reject this possibility.

To examine the distribution of CT cells, two statistical tests were performed. The distribution failed to conform to a random Poisson distribution ($\alpha = 0.005$, χ^2 test), as well as a uniform distribution ($\alpha = 0.005$, χ^2 test). We, therefore, concluded that the CT cells were clustered in group 1.

DISCUSSION

Cluster analysis classification of layer 5 neurons

We present a morphologic classification of layer 5 cells from mouse primary visual cortex, based on strict quantitative criteria. We reconstructed the morphologies of 158 neurons three-dimensionally by using three staining methods. A series of morphologic variables was measured, and the cells were classified based on their somatic and dendritic morphologies. To reach an objective classification, two statistical methods were applied sequentially to the quantitative data obtained from the reconstructions. Initially, principal component analysis was used to select the variables that accounted for most of the variance in the data set and, therefore, better represented differences among different cell types. Then, cluster analysis was used to group cells on the basis of morphologic similarity.

The cells analyzed in this study fall into two broad classes, based on the presence or absence of an apical tuft in layer 1. The first main group includes all the large pyramidal neurons with apical dendrites that form an extensive tuft immediately below the pia mater. The second main group can be subdivided into four distinct groups. The first of these includes polarized nonpyramidal neurons whose dendrites do not branch symmetrically around the cell body and short pyramidal neurons with apical dendrites that reach no further than layer 3. We find a group of pyramidal neurons that extend to the upper cortical layers but have much less elaborate dendritic trees compared with the cells of the leftmost branch (branch 1) of the dendrogram. Most of the small cells of our data set form a distinct class. Finally, we find a group that includes short pyramidal cells with a high number of primary dendrites, cells with fewer dendrites and less elongated dendritic arbors, and atypically oriented cells, i.e., cells with a nonperpendicular orientation with respect to the cortical layers.

Methodologic considerations

Because this study is one of the first to use cluster analysis for the morphologic classification of neurons, it is appropriate to discuss certain ways of validating its results and overcoming some of its potential weaknesses. First of all, our study is purely morphologic and no direct information about the function of the different cell classes is provided. Further experiments are obviously required to elucidate the functional roles of the cell types described. In this respect, physiological measurements can be used in conjunction with anatomic measurements to perform a combined anatomic–physiological cluster analysis. Another potential improvement to our study would be the inclusion of the axonal morphologies. Due to variable success rates in the recovery of axonal morphology, which could compromise the quantitative classification, this study focused exclusively on dendritic morphology.

To reduce bias due to a specific method for visualization of neuronal morphology, three widely different staining techniques were used. Intracellular biocytin injections allow the complete reconstruction of neurons, often including the axons, combined with the physiological characterization of the stained cells, but are restricted by the limitations of whole-cell recording. In this technique, there is a bias in staining cells that are larger and closer to the surface of the slice. Indeed, this finding is evident by

the highest percentage of intracellularly injected neurons in group 1, which includes the largest cells in this study. On the other hand, the Golgi and DiOlistics methods are more random and more efficient in the sense that a large number of cells can be stained and reconstructed in each section.

One potential problem is that the cluster analysis would classify cells on the basis of staining techniques. Although one cannot rule out this possibility completely, technical biases are not considered significant because our groups are composed of cells visualized according to at least two staining protocols. Specifically, group 1 had 35 biocytin and 12 DiOlistics cells, group 2 had 2 and 25, group 3 had 7 and 15, group 4 had 1 and 5, and group 5 had 8 and 43, respectively. Golgi-impregnated cells were found only in groups 2 and 3. However, this finding should not be interpreted as a technical bias, because only a small number of these cells (5 of 158) is included in the analysis. Therefore, we argue that, at least for the case of biocytin and DiOlistics techniques, the morphologies of the reconstructed neurons are not systematically different.

The CT cells included in our analysis are used as a control for our classification, because they are considered to form a relatively homogeneous population of neurons. The basis of this homogeneity is as follows: (1) CT cells project to the same subcortical target, i.e., superior colliculus; (2) CT cells have similar intrinsic electrophysiological firing patterns; and (3) CT cells show very similar dendritic morphologies (Schofield et al., 1987; Kasper et al., 1994; Kozloski et al., 2001). Most CT cells included in the analysis are members of the first main group of tall pyramidal neurons. By using two statistical tests described in the Results section, we show that the CT neurons are neither randomly nor uniformly distributed but are clustered within the population. This finding was predicted based on the known morphology of these cells. However, a few (7 of 27) CT neurons were classified in other groups. We believe that these neurons represent cases where there has been an underestimation of the apical dendrite due to incomplete staining. Similarity among the basal regions of these neurons is the most likely reason for their inclusion in other groups.

The labeling techniques applied in this study also allow the visualization of dendritic spines. However, quantitative information about the spines was not included in the analysis due to the high variability in spine density that could result in inaccurate measurements and counts. Only a few general statements about the distribution of spiny and aspiny neurons can be made: the vast majority of the neurons of groups 1 and 3 were spiny, all the cells of group 4 lacked dendritic spines, and the remaining two groups included both spiny and aspiny cells.

Comparison with previous studies

Numerous studies on classification of neurons in various parts of the nervous system have been reported; however, they have been for the most part qualitative (Ramón y Cajal, 1904; Lorente de Nó, 1922; Peters and Jones, 1984). In general, neurons are classified morphologically based on either the dendritic arbor or the axonal projection patterns. Our analysis classifies neurons based on extensive and precise measurements of somata and dendritic arbors. In a widely cited study, Peters and Kara distinguish two types of pyramidal neurons in Golgi-impregnated rat primary visual cortex: large and medium (Peters and Kara, 1985a). The reported neuronal types are similar to the subgroups of tall pyramidal neurons that we find in group 1, specifically with respect to the shapes and sizes of cell bodies and the branching patterns of the apical dendrites. However, in the Peters and Kara study, apical dendrites are thicker. They also describe three types of nonpyramidal cells: bipolar, smooth or sparsely spiny multipolar, and chandelier cells (Peters and Kara, 1985b). With the exception of chandelier cells, which we did not encounter, nonpyramidal neurons in our study show similar features; however, they do not form distinct classes.

Traditionally pyramidal neurons are divided into classic pyramids, whose apical dendrites reach layer 1, and the ones that terminate in deeper cortical layers. According to Lorente de Nó, the latter group is further subdivided into medium and short or star pyramids. Based on this terminology, medium pyramids have apical dendrites that reach no further than layer 4, whereas the dendritic arbors of the short pyramids are restricted to layer 5 (Lorente de Nó, 1949). In our study, these two subdivisions are collectively referred to as short pyramidal neurons. On the other hand, our classification distinguishes between two subgroups of the classic pyramids: wide and narrow tufted tall pyramidal neurons.

The pyramidal cells with "dangling" basal dendrites seen in class 2A (Fig. 5A) have not been reported in the past. These cells have small conical somata and short apical dendrites. The basal dendrites do not branch laterally but reside exclusively opposite to the apical dendrite, extending ventrally toward layer 6. These neurons were visualized with all three staining methods and were shown to be monosynaptically connected to CT cells (Kozloski et al., 2001).

Neurons have also been classified according to the axonal arborization patterns. Originally, Cajal defined long-axon and short-axon neurons (Ramón y Cajal, 1891, 1892). Long-axon neurons resemble the tall pyramidal neurons described in our study (class 1). Short-axon neurons show a large variety of neuronal morphologies, including certain pyramidal neurons, small basket cells, and chandelier cells. Due to incomplete axonal reconstruction, certain classes of neurons that could otherwise be distinguished were not defined as such in our study.

Future directions

A logical continuation to the morphologic classification would be the elucidation of the potential function of the classes described. Electrophysiological recordings from neurons labeled with the DiOlistics method could provide physiological data on cell types that might not have been selected otherwise. Immunocytochemistry in combination with single cell biocytin injections or DiOlistics can provide information about the chemical properties of specific cell types, such as calcium-binding proteins or neurotransmitters. Such experiments could provide information on the relationship between neuronal morphology and function.

In contrast to the application of subjective criteria, the use of quantitative variables and mathematical methods to describe and classify neurons allows one to compare results from studies in different parts of the nervous system or at different developmental stages. In addition, considering the powerful tools of mouse genetics, the morphologic effects of gene expression manipulations can be

studied in an objective manner. For example, changes in the classification dendrogram may reflect the effects of the level of expression of a certain protein on the morphology of a neuron.

The objective morphologic description of neurons provides an important step toward understanding cortical circuits. To this end, defining the cell types, their properties and interconnections is crucial for reconstructing the basic structural elements of the nervous system. The combination of anatomic, physiological, and biochemical studies will provide great insight to the understanding of the function of the nervous system.

ACKNOWLEDGMENTS

We thank James Kozloski for the sample of corticotectal neurons, Sila Konur and Noelia Weisstaub for the Golgi samples, Knut Holthoff and Bu-Qing Mao for help, and members of the laboratory for comments.

LITERATURE CITED

Cattell R. 1966. The scree test for the number of factors. Multivar Behav Res 2:245–276.

Cauli B, Porter JT, Tsuzuki K, Lambolez B, Rossier J, Quenet B, Audinat E. 2000. Classification of fusiform neocortical interneurons based on unsupervised clustering. Proc Natl Acad Sci U S A 97:6144–6149.

Crick FHC, Asanuma C. 1986. Certain aspects of the anatomy and physiology of the cerebral cortex. In: McClelland JL, Rumelhart DE, editors. Parallel distributed processing. Cambridge: MIT Press. p 333–371.

Douglas RJ, Martin KAC. 1998. Neocortex. In: Shepherd GM, editor. The synaptic organization of the brain. Oxford: Oxford University Press. p 459–511.

Gallyas F. 1979. Silver staining of myelin by means of physical development. Neurol Res 1:203–209.

Gan WB, Grutzendler J, Wong WT, Wong RO, Lichtman JW. 2000. Multicolor "DiOlistic" labeling of the nervous system using lipophilic dye combinations. Neuron 27:219–225.

Gilbert CD, Wiesel TN. 1983. Clustered intrinsic connections in cat visual cortex. J Neurosci 3:1116–1133.

Gupta A, Wang Y, Markram H. 2000. Organizing principles for a diversity of GABAergic interneurons and synapses in the neocortex. Science 287:273–278.

Hallman L, Schofield B, Lin C. 1988. Dendritic morphology and axon collaterals of corticotectal, corticopontine, and callosal neurons in layer V of primary visual cortex of the hooded rat. J Comp Neurol 271:149–160.

Hess DT, Merker BH. 1983. Technical modifications of Gallyas' silver stain for myelin. J Neurosci Methods 8:95–97.

Kaiser HF. 1960. The application of electronic computers to factor analysis. Educ Psychol Measure 20:141–151.

Kasper E, Larkman A, Lubke J, Blakemore C. 1994. Pyramidal neurons in layer 5 of the rat visual cortex. I. Correlation among cell morphology, intrinsic electrophysiological properties, and axon targets. J Comp Neurol 339:459–474.

Katz LC, Burkhalter A, Dreyer WJ. 1984. Fluorescent latex microspheres as a retrograde neuronal marker for in vivo and in vitro studies of visual cortex. Nature 310:498–500.

Kolb H, Fernandez E, Schouten J, Ahnelt P, Linberg KA, Fisher SK. 1994. Are there three types of horizontal cell in the human retina? J Comp Neurol 343:370–386.

Kozloski J, Hamzei-Sichani F, Yuste R. 2001. Stereotyped position of local synaptic targets in neocortex. Science 293:868–872.

Lorente de Nó R. 1922. La corteza cerebral del ratón. Trab Lab Invest Bio (Madrid) 20:41–78.

Lorente de Nó R. 1949. Cerebral cortex: architecture, intracortical connections, motor projections. In: Fulton JF, editor. Physiology of the nervous system. New York: Oxford University Press. p 288–330.

Lund JS. 1988. Anatomical organization of macaque monkey striate visual cortex. Annu Rev Neurosci 11:253–288.

MacNeil MA, Heussy JK, Dacheux RF, Raviola E, Masland RH. 1999. The shapes and numbers of amacrine cells: matching of photofilled with Golgi-stained cells in the rabbit retina and comparison with other mammalian species. J Comp Neurol 413:305–326.

Majewska A, Yiu G, Yuste R. 2000. A custom-made two-photon microscope and deconvolution system. Pflugers Arch 441:398–409.

Marcoulides GA, Hershberger SL. 1997. Multivariate statistical methods: a first course. Mahwah, NJ: Lawrence Erlbaum.

Martin KAC, Whitteridge D. 1984. Form, function and intracortical projections of spiny neurones in the striate visual cortex of the cat. J Physiol 353:463–504.

Miller MW. 1988. Development of projection and local circuit neurons in neocortex. In: Peters A, Jones EG, editors. Development and maturation of cerebral cortex. Cerebral Cortex 7. New York: Plenum. p 133–166.

Miller MW. 1988. Maturation of rat visual cortex: IV. The generation, migration, morphogenesis, and connectivity of atypically oriented pyramidal neurons. J Comp Neurol 274:387–405.

Mountcastle VB. 1998. Perceptual neuroscience: the cerebral cortex. Cambridge: Harvard University Press.

Nadol JB Jr, Burgess BJ, Reisser C. 1990. Morphometric analysis of normal human spiral ganglion cells. Ann Otol Rhinol Laryngol 99:340–348.

Peters A, Jones EG. 1984. Cerebral cortex. New York: Plenum.

Peters A, Kara DA. 1985a. The neuronal composition of area 17 of rat visual cortex. I. The pyramidal cells. J Comp Neurol 234:218–241.

Peters A, Kara DA. 1985b. The neuronal composition of area 17 of rat visual cortex. II. The nonpyramidal cells. J Comp Neurol 234:242–263.

Ramón y Cajal S. 1891. Sur la structure de l'ecorce cérébrale de quelques mammifères. La cellule 7:125–176.

Ramón y Cajal S. 1892. El Nuevo concepto de la histologia de los centros nerviosos. Rev Ciencias Med 18:457–476.

Ramón y Cajal S. 1904. La Textura del Sistema Nerviosa del Hombre y los Vertebrados. Madrid: Moya.

Romesburg HC. 1984. Cluster analysis for researchers. Belmont, CA: Lifetime Learning.

Schofield B, Hallman L, Lin C. 1987. Morphology of corticotectal cells in the primary visual cortex of hooded rats. J Comp Neurol 261:85–97.

Sholl DA. 1956. The organization of the cerebral cortex. New York: John Wiley.

Solnick B, Davis T, Sterling P. 1984. Numbers of specific types of neuron in layer IVab of cat striate cortex. Proc Natl Acad Sci U S A 81:3898–3900.

Somogyi P, Tamas G, Lujan R, Buhl E. 1998. Salient features of synaptic organization in the cerebral cortex. Brain Res Brain Res Rev 26:113–135.

Stevens CF. 1998. Neuronal diversity: too many cell types for comfort? Curr Biol 8:R708–710.

Strausfeld NJ. 1980. The Golgi method: its application to the insect nervous system and the nomenon of stochastic impregnation. In: Strausfeld NJ, Miller TA, editors. Neuroanatomical techniques. New York: Springer. p 131–203.

Szentagóthai J. 1978. The neuron network of the cerebral cortex: a functional interpretation. Proc R Soc Lond B 201:219–248.

Tamas G, Buhl EH, Lorincz A, Somogyi P. 2000. Proximally targeted GABAergic synapses and gap junctions synchronize cortical interneurons. Nat Neurosci 3:366–371.

Wiser AK, Callaway EM. 1996. Contributions of individual layer 6 pyramidal neurons to local circuitry in macaque primary visual cortex. J Neurosci 16:2724–2739.

Zhang H, Yu CY, Singer B, Xiong M. 2001. Recursive partitioning for tumor classification with gene expression microarray data. Proc Natl Acad Sci U S A 98:6730–6735.